Investigation of Limit State Behavior of Post-Tensioned Steel Beam-to-Column Connections

Sedef Kocakaplan[1], Anne Hulsey[2], Patricia Clayton[3]

[1] Ph.D. Candidate, Department of Civil, Architectural and Environmental Engineering, University of Texas at Austin - Austin, TX, USA.
[2] Ph.D. Candidate, Department of Civil and Environmental Engineering, Stanford University- Stanford, CA, USA.
[3] Assistant Professor, Department of Civil, Architectural and Environmental Engineering, University of Texas at Austin – Austin, TX, USA.

ABSTRACT

Self-centering moment resisting frames with post-tensioned (PT) beam-to-column connections have been proposed as a damage-mitigating alternative to conventional steel moment-resisting frames used in seismic force-resisting structural systems. The self-centering capability of properly designed PT connections proves to be an effective tool for improving resilience of a building following an earthquake; however, the rocking behavior of PT beam-to-column connections could result in excessive compressive forces at the contact surfaces between beams and columns. These concentrated compressive forces can cause local buckling at beams, which causes plastic shortening of the beam and loss of connection moment-resisting capacity. A computational study was performed using finite element methods to investigate this local buckling behavior. The finite element models were validated using experimental data from quasi-static tests of steel PT moment-resisting connections conducted at the University of Texas at Austin. This paper focuses on comparison of the finite element model and the experimental results in terms of capturing local buckling behaviors in steel PT moment-resisting connections.

Keywords: Moment-resisting frames, Post-tensioned steel beam-to-column connections, Self-centering, Finite element analysis, Local buckling

INTRODUCTION

Compared to conventional moment resisting frames, which are designed to dissipate energy under seismic loads through yielding of main structural members, self-centering steel moment resisting frames with post-tensioned (PT) beam-to-column connections were proposed by Ricles et al. [1] to prevent damage to structural members and reduce permanent deformations in the structure. PT beam-to-column connections constitute post-tensioned tendons within the beams that are anchored behind the column flanges. As the connection moment demand increases, PT connections are allowed to rock about their flanges, creating a gap between the beam and column. This rocking behavior allows structural members to stay essentially elastic under earthquake loads, while energy dissipation is provided by the special energy dissipation devices. These energy dissipation devices can be yielding elements within the connection (e.g. angles in Garlock [2], bucking-restrained bars in Christopoulos et al. [3]), friction devices (e.g. flange or web friction devices in Iyama et al. [4] and Lin et al. [5], respectively), or even yielding elements outside of the connections (e.g. steel plate shear walls per Clayton et al. [6]). Additionally, its self-centering capability provides a restoring force to return the PT connection to its original position after an earthquake, thus resulting in near zero residual story drifts.

These PT forces in the connection create a compressive force at contact surfaces between the beam and column. These contact forces increase in the compression flanges after gap opening in the connection, which can lead to local buckling. Local buckling causes shortening in beam length, resulting in loss of post-tension force and subsequently reducing connection capacity and self-centering capability of the structure [2]. For this reason, local buckling is a critical limit state that should be considered in design of self-centering steel moment-resisting frames. Additionally, even in well-designed PT connections that can withstand local buckling under design earthquake levels, it is necessary to understand the strength degrading behaviors associated with beam local buckling for assessing collapse risk of these systems.

A considerable amount of studies has been performed related to seismic behavior of self-centering steel PT beam-to-column connections, several of which have addressed the beam local buckling limit state. Garlock [2] conducted several experiments in which drifts were applied up to specimens' ultimate capacity to investigate the limit states for this type of connections. They showed that high compressive stress concentrations occurred at the end of the flange reinforcing plates and defined strains that led to beam local buckling based on measured strain gauge readings at this location. Garlock [2] categorized strains leading to

local buckling as (i) the "strain rise" at which strains no longer follow the projected path of previous cycles and (ii) the strain associated with the peak post-tension force. They demonstrated that strain rise occurs with an average of $2\varepsilon_Y$, where ε_Y is the yield strain of the beam material. Subsequently, they concluded that to limit beam local buckling at the Maximum Considered Earthquake (MCE) level, the strain level should be limited at $2\varepsilon_Y$ at Design Basis Earthquake (DBE) level. Following this research, experimental tests by Chou et al. [7] showed that strain rise occurs at $1.4\varepsilon_Y$, while Chou et al. [8] showed that strain rise at beam flange can reach up to $6\varepsilon_Y$ without buckling by using web stiffeners. Lastly, Hulsey [9] studied PT beam-to-connections to address whether with-to-thickness ratios given in design specifications are applicable for the self-centering moment resisting frame systems. They conducted experiments with beams with varying cross sections. Test results demonstrated that beams with higher flange width-to-thickness $(b_f/2t_f)$ ratios buckled at much lower strains compared to beams with lower flange $b_f/2t_f$ ratios. They suggested that additional experimental analysis should be performed, and finite element modeling of these connections should be conducted to establish an appropriate value for the limit of width-to-thickness of beam flanges as well as webs in PT connections.

As suggested by Hulsey [9], finite element (FE) analyses can provide insight into the beam local buckling limit state behavior of PT beam-to-column connections. Past research has been performed to develop FE models of these connections. To fully capture the cyclic response of self-centering moment resisting frames, Kim and Christopoulos [10] conducted FE analyses using solid (continuum) elements. The FE results compared well with the experimental tests performed by Kim and Christopoulos [10] for capturing the cyclic behavior of self-centering moment resisting frames with beam local buckling. Another researcher, Moradi et al. [11], used solid element FE models to simulate the behavior of PT steel connections with bolted yielding angles tested by Ricles et al [1]. Furthermore, Ahmadi et al. [12] used FE models of PT connections with bolted yielding angles to study seismic collapse resistance of self-centering moment resisting frames. The FE models were employed in incremental dynamic analyses. Their models consist of shell elements in regions near the beam ends, where local buckling may occur, and the local buckling behavior was calibrated against the experiments conducted by Garlock [2]. They demonstrated that FE models can predict the local buckling of beams accurately, and they stated that the accurate modeling of beam local buckling is crucial to obtain proper assessment of the self-centering moment resisting frame's collapse resistance.

The main purpose of this paper is to further study beam local buckling limit state for PT beam-to-column connections under cyclic loads. Specifically, this paper presents the development and validation of FE models of steel PT beam-to-column connections. The Abaqus finite element program [13] is used to model the PT beam-to-column connections, and the model is validated using results from experiments conducted by Hulsey [9]. These validated FE models are being used in ongoing computational parametric studies (not discussed in this paper) to investigate local beam buckling behaviors and the effects of the flange width-to-thickness ratios for these connections. Details of the experimental tests, the FE model, and comparison of the experimental and computational results are provided in the following sections.

REFERENCE EXPERIMENTS

In this study, the experiments performed by Hulsey [9] were selected to validate the finite element models. To isolate beam local buckling behavior, they conducted experiments with a single beam-to-column connection. Additionally, energy dissipating devices were not included in these experiments. A total of three specimens were tested with varying beam dimensions, and subsequent PT diameters, tension forces in PT bars, and reinforcing plate thicknesses. Each specimen consisted of a beam with two PT bars located on each side of the beam web, which are connected to a column, as shown in Figure 1a. The specimens were loaded cyclically via an actuator as shown in Figure 1a. The first test consists W18x65 beam, PT bars with a 46 mm (1 ¾ inch) diameter and reinforcing plates with a thickness of 12.7 mm (0.5 inch). The width-to-thickness ratios of this beam are $b_f/2t_f = 5.06$ for flange and $h/t_w = 37.4$ for web. In this specimen, the east and west bars were tensioned to 832 kN (187 kips) and 823 kN (185 kips), respectively, for a total of 1654 kN (372 kips). The second test used a W18x55 section with slightly higher width-to-thickness ratios, which are $b_f/2t_f = 5.98$ for flanges and $h/t_w = 43.2$ for webs. The reinforcing plates were 19.05 mm (0.75 inch) thick and PT bars were 46 mm (1 ¾ inch) diameter. The bars had an initial tension of 781 kN (175.5 kips) and 776 kN (174.5 kips), for a total of 1557 kN (350 kips). The final test had a W18x76 beam with a larger area compared to previous specimens, therefore a larger PT bar with a 57 mm diameter (2 ¼ inch) was used. The width-to-thickness ratios of beam are $b_f/2t_f = 8.11$ for flange and $h/t_w = 39.6$ for web. The reinforcing plates were 12.7 mm (0.5 inch) thick and the east and west PT bars were tensioned to 738 kN (166 kips) and 758 kN (170.5 kips) for a total of 1496 kN (336.5 kips). The length of the beams in first two experiments were 3.67 m (144.5 inch) with the actuator loading at 3.09 m (121.75 inch) from the column face, while the beam that was used in last experiment was 3.06 m (120.5 inch) with the actuator loading at 1.87 m (73.75 inch) from the column face. The purpose of changing the beam length and actuator location in the last specimen was to increase the drift capacity from 5% to 10% drift. The summary of the test specimens' properties is provided in Table 1.

Table 1. Summary of Test Specimens Properties

Specimen Number	Beam Size	Reinforcing Plate Thickness	PT Diameter	Initial PT Force		$b_f/2t_f$	h/t_w
				East	West		
1	W18x65	12.7 mm	46 mm	832 kN	823 kN	5.06	37.4
2	W18x55	19.05 mm	46 mm	781 kN	766 kN	5.98	43.2
3	W18x76	12.7 mm	57 mm	738 kN	758 kN	8.11	39.6

A W12x120 column with a length of 3.962 meters (13 ft) was attached to the strong floor via an anchor column (shown as blue in Figure 1a) at tie-down locations 3.658 meters (12 ft) apart. The lateral bracing was located at 344.81 cm (135.75 inch) above the column face for specimen number 1 and 2 while it is located at 271.15 cm (106.75 inch) above the column face for specimen number 3. The connections include two PT bars on each side of the beam web, which were anchored at the lower anchor column and at an anchorage assemble at top of the specimen as shown in Figure 1a. The anchorage assembly consists two 381x 508 mm (15x20 inch) size plates with a thickness of 50.8 mm (2 inch) and they were separated by four 50.8 mm (2 inch) tall and 25.4 mm (1 inch) wide "webs". The columns had 50.8 mm (2 inch) stiffeners located in line with the beam flanges so that the compression forces from the beam had a direct load path to the strong floor [9]. The length of the reinforcing plates for all specimens were equal to the nominal beam depth, d= 203.2 mm (18 inch) and their thickness varies with beam geometry as shown in Table 1. As suggested by Ricles et al. [14], a 50.8 mm (2 inch) wide bearing plate was welded to the end of each beam flange and reinforcing plate to provide an even contact surface with column face.
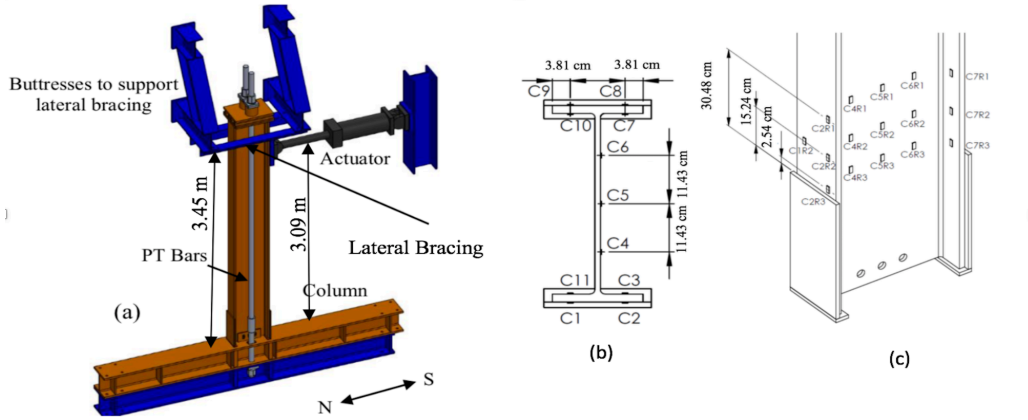

Figure 1. (a) Test Setup shown for Specimen 2, and (b, c) strain gauge locations, Hulsey [9].

Reinforcing plates, stiffeners, bearing plates were made of steel with a nominal yield strength of 345 MPa (50 ksi), while the PT bars were made of high strength steel with an ultimate strength of 1034 MPa (150 ksi) in compliance with ASTM A722 specifications. Columns and beams were made of A992 steel material, represented as SM (structural steel material) in Figure 2b. To define material properties for beams, coupon tests were conducted at the Ferguson Structural Engineering Laboratory. Tri-linear constitutive relationships were defined for each beam material as shown in Figure 2c and in Table 2.

Table 2. Material Properties for Beam in Specimen 2

Beam Size	σ_Y (MPa), ε_Y	σ' (MPa), ε'	σ_U (MPa), ε_U
W18x55-Web	405, 0.002	500, 0.048	537, 0.251
W18x55-Flange	362, 0.0018	474, 0.049	547, 0.150

The loading sequence was based on the AISC Seismic Provisions (2010), [15] requirements for beam-to-column. However, to reduce the computational demands, the number of cycles in the elastic range were reduced, resulting in the loading sequence as follows: 1 cycle at 0.375% drift, 4 cycles at 0.5% drift and 2 cycles at 0.75%,1%,1.5%,2%,3%,4%,5%. (increasing at 1% drift increments up to 9% drift for final specimen).

Finally, beams were instrumented with strain gauges above the reinforcing plates to measure the strains in the area where local buckling was expected. These strain gauges were located in three different "rows" above the end of the reinforcing plate as shown in Figure 1b.
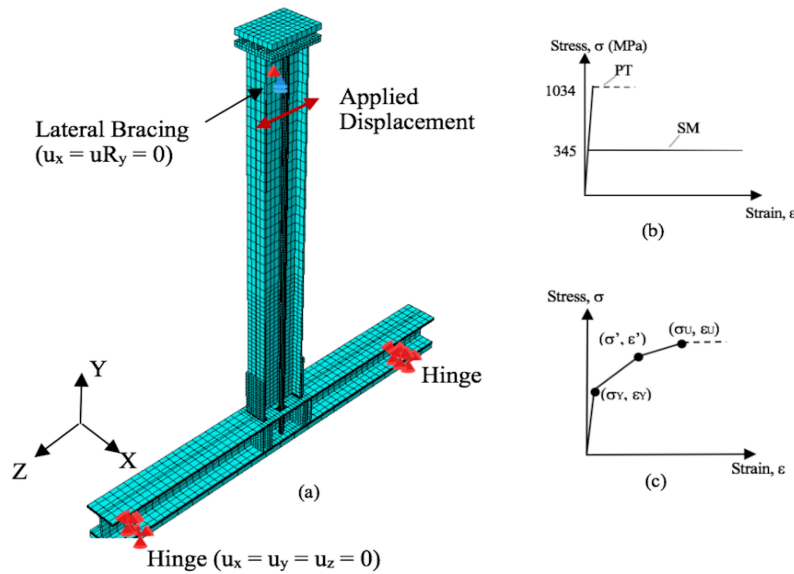

Figure 2. (a) Mesh Detail of the Abaqus Models, (b) A992 Steel and PT Materials, (c) Beam Material.

FINITE ELEMENT MODELS

Abaqus Finite Element software is used to study the PT beam-to-column connections. Three-dimensional solid (continuum) elements are employed to model the beam, column, PT elements, reinforcing plates and stiffeners. Tri-linear kinematic hardening models are adopted for the beam material as given in Table 2 based on the coupon test results for Specimen 2. All other materials were defined using nominal yield strengths and remained essential elastic during the analyses. Abaqus requires material input to be in terms of true stress and true strain; therefore, engineering stress and strain results from the coupon tests are used to calculate true strain and stress values for the beam material.

To model interactions between welded components (e.g. between the beam and the reinforcing plates and bearing plates, etc.), tie constraints are employed. To define contact interaction between bearing plates and column face, surface-to-surface contact interaction is used. Contact behavior on Abaqus is simulated through tangential and normal behavior between the contact surfaces. The normal behavior is defined by hard contact, while the tangential behavior is simulated by penalty method with a friction coefficient of 0.33, as suggested by Moradi et al [12]. The columns consist of pin supports at tie-down locations. The beams are laterally supported at the same locations as the experiments and a rigid body constraint is defined to assign these conditions. Lateral displacement is also applied at the same location as the actuator using the same load protocol used in the tests. Finally, prestress loads are defined through the bolt load property in Abaqus, as suggested by Esposto [16].

Abaqus employs master-slave formulation for tie constraint and for contact interactions. Meshing for these surfaces should be performed carefully to prevent convergence problems, as the mesh on the slave surface should be denser than its master surface. Finer meshes are also assigned at beam parts closer to the contact surface of beam and column as shown in Figure 2a. Abaqus analyses are performed in two steps. First, preloads are generated in the PT bars, then cyclic displacement are applied to the system via a nonlinear static analysis considering geometric and material nonlinearity.

NUMERICAL RESULTS AND DISCUSSION

Global Response Results

The results from the experimental tests are compared with the finite element results. Due to space limitations, detailed results from only one specimen, the W18x55 beam, will be shown in this paper. Figure 3 shows the moment-drift response and PT force-drift response comparisons for the W18x55 specimen. As shown in Figure 3, as similarly observed for the other specimens not shown in this paper, the global response for the specimens are well represented by the computational models. In general

PT connections without added energy dissipation devices exhibit a bilinear elastic behavior. When local buckling occurs at large drift demands, the beam shortens, resulting in a loss of PT force and a reduced connection moment capacity, as is indicated by the softening behavior and the hysteresis in the global moment-drift response cycles at 3% drift in Figure 3a. In general, the FE models are able to capture the global behavior of the connections including initial stiffness, decompression moment, post yield stiffness, and PT force loss and moment strength degradation after the occurrence of local buckling.
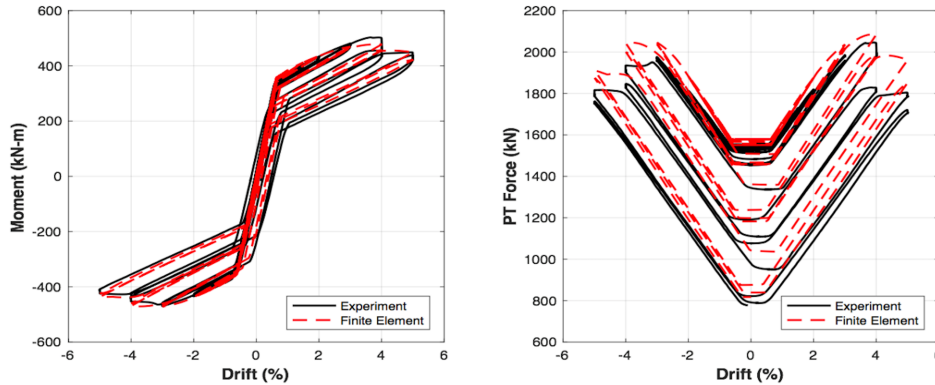
Figure 3. Specimen with W18x55 Beam (a) Moment Response and (b) PT Force

As shown in Figure 3, the computational results for the specimen with the W18x55 beam captures the cyclic response of the experiment. Decompression occurs between 0.6 % and 0.75 % for both experimental and computational models, respectively. As shown in Figure 3b, the FE model generally captures the PT behavior and losses observed in the experiment. As expected, the PT force remains relatively constant at low drift levels prior to decompression and increases linearly following connection decompression. The experiment exhibited minor PT losses up to 2% drift, which are believed to be due to anchorage seating and were not captured in the FE model. During the drift cycle up to 4% drift, both the experimental specimen and the FE model exhibit significant softening in the moment-drift and PT-drift responses. The PT forces reach their maximum values at 4% drift, resulting in maximum PT forces of 1935 kN in the specimen and 2042 kN in the FE model (the difference of experimental and computational results is ~5%). Corresponding to this softening response, some minor flange local buckling was observed at the edge of the north flange over a length of approximately 23 cm beyond the end of the reinforcing plate, and local buckling in web was also reported as shown in Figure 4. The buckling that began in the 4% drift cycle continued to grow and resulted in strength degradation up to 5% drift as shown in Figure 3a. The FE model successfully captured the strength degradation behavior, including the total PT loss after unloading from 5% drift and the peak connection moment capacity in the 5% cycle.
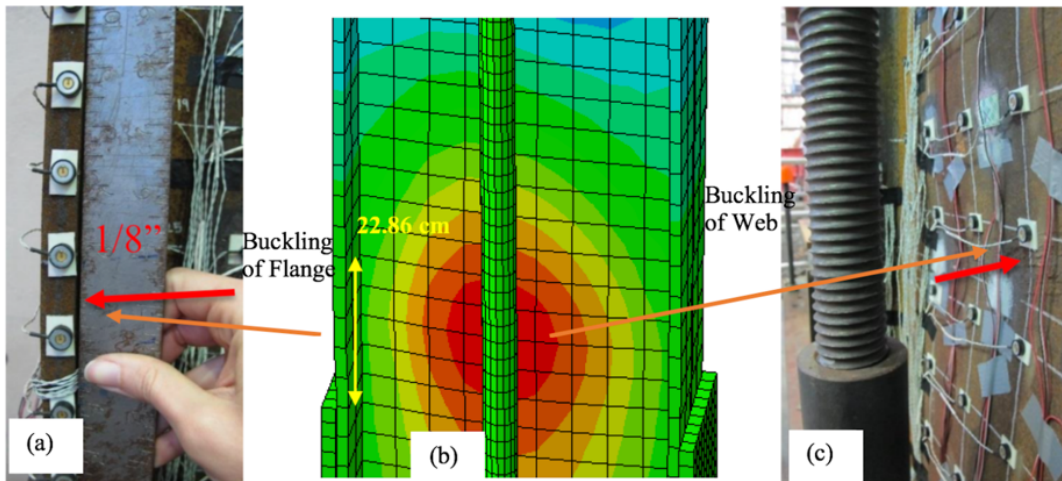

Figure 4. Specimen with W18x55 beam, web and flange buckling at first 4% South peak, (a) flange buckling in experiment [9], (b) computational model flange and web buckling, and (c) web buckling in experiment [9]

Strain Data and Buckling Results

Hulsey [9] analyzed the strain gauge data using methods similar to the ones employed in Garlock [2] and Chou [7,8]. The focus in this work was on flange buckling, and the design procedure proposed by Garlock [2] indicated flange buckling should happen before web buckling; thus, only flange strain results will be discussed. Instances of "strain rise" were defined in both Garlock [2] and Hulsey [9] as cycles where the strains during unloading did not return along the same path as during the loading, as shown in Figure 5 a and b. During their experiments, Garlock [2] detected that the strain rise is a precursor to observable buckling, which is characterized in Figure 5 by excessively large increases in compressive strains. In addition to this, they reported that strain rise happens at strains between 0.9 to 2.5 ε_y, at an average of 2 ε_y. However, one strain gauge result from Garlock's tests [4], shown in Figure 5b, resulted in a strain rise that was not immediately followed by buckling behavior. Finally, Garlock recommended that to prevent buckling at the MCE level, the strain rise should be limited to 2 ε_y at the end of the reinforcing plate for the DBE level.
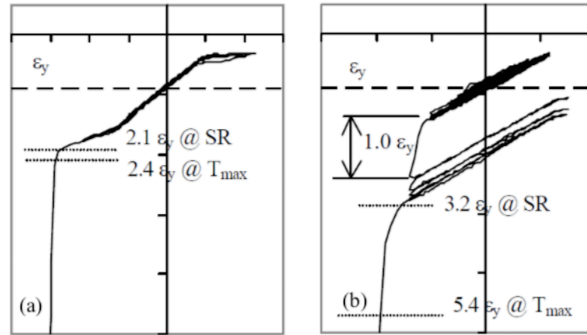

Figure 5. Strain Rise Results from Garlock [2] (a) Typical Example of Strain Rise (b) Example of pre-buckle strain rise.

Hulsey [9] compared the experiments strain rise results with the Garlock's observations. Hulsey [9], located the strain gauges at the locations on both beam flanges and webs where beam local buckling can be detected as shown in Figure 1 b and c. In this section we compared our strain results from the finite element models with the referred experimental results. Again, only results from first two specimens were include due to space limitations.
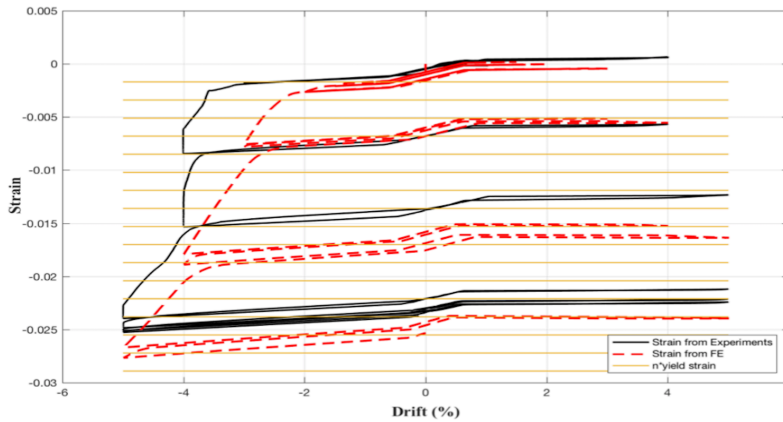

Figure 6. Comparison of strain data for Specimen 2 beam from strain gauge C1R2 that is on north flange

Strain gage vs. drift results for the W18x55 specimen is shown in Figure 6. The C1R2 strain gauge located on the north flange approximately 15.25 cm from the end of the reinforcing plate, as shown in Figure 1c, was selected as it is closest to the middle of the buckling observed in the north beam flange as shown in Figure 4. Strain data from the FE model was selected from mesh points close to, within 0.76 mm, of the strain gage location in the experiment. According to Figure 6, the FE model and the experiment exhibit their initial strain rise at a similar strain level, between $1\varepsilon_y$ to $2\varepsilon_y$ (ε_y in Figure 6 is calculated according to nominal yield strength). Furthermore, at each subsequent cycle of loading after the initial strain rise the amplitude of strain rise

is similar in experiment and FE model, resulting in similar peak strains at the end of testing. The main difference between the FE model and experiment is that the FE model exhibits its initial strain rise during the 3% drift cycle, and the experimental specimen exhibits its initial strain rise during the 4% drift cycle suggesting that the beam flanges in the computational models start to buckle at lower drifts than the experimental models. However, due to the relatively coarse mesh of the experimental strain gages, the experimental strain results may not capture the ideal location of buckling initiation.

CONCLUSIONS

 PT beam-to-column connections have been proposed to provide self-centering capability and energy dissipation through specially designed energy dissipation devices. One of the main concerns in PT connections is the concentration of compressive stresses due to contact forces at the connection surfaces. The contact forces can lead to beam local buckling, which results in PT force losses and subsequent reduction in connection flexural capacity and self-centering capability. Past PT connection experiments by Garlock [2] and Chou [6,7], along with recent tests conducted by Hulsey [9], have shown experimental results for specimen with local buckling; however, the total number of test specimens investigating the local buckling limit state is limited. Therefore, computational studies can be used to further explore local buckling behaviors for a wider range of design parameters. To this end, this paper presents a PT connection finite element model that is validated with experimental results from Hulsey [9]. The results presented in this paper focus on responses associated with local buckling, including PT losses and strain rises in the region of local buckling. Ongoing research and computational parametric studies investigating local buckling behaviors in a wide range of PT connections using this validated FE model will be presented in future publications.

ACKNOWLEDGMENTS

REFERENCES

[1] Ricles, J., Sause, R., Garlock, M., & Zhou, C. (2001). "Posttensioned seismic resistant connections for steel frames". *Journal of Structural Engineering*, 127(2), 113–121.

[2] Garlock, M. E. M. (2002). *Design, analysis, and experimental behavior of seismic resistant post-tensions steel moment resisting frames*. Doctoral Dissertation, Leigh University, Bethlehem, PA.

[3] Christopoulos, C., Filiatrault, A., Uang, C., & Folz, B. (2002). "Posttensioned energy dissipating connections for moment-resisting frames". *Journal of Structural Engineering*, 128(9), 1111-1120.

[4] Iyama, J., Seo, C-Y., Ricles, J.M., Sause, R. (2008). "Self-centering MRFs with bottom flange friction devices under earthquake loading". *Journal of Constructional Steel Rese*arch, 65(2), 0143-974.

[5] Lin, Y., Sause, R., & Ricles, J.M. (2013). "Seismic performance of steel self-centering, moment-resisting frame: Hybrid simulations under design basis earthquake". *Journal of Structural Engineering*, 139(11), 1823-1832.

[6] Clayton, P.M., Berman, J.W., & Lowes, L.N. (2012). Seismic design and performance of self-centering steel plate shear walls. *Journal of Structural Engineering*, 138(1), 22-30.

[7] Chou, C., Chen, J., Chen, Y., & Tsai, K. (2006). "Evaluating performance of post-tensioned steel connections with strands and reduced flange plates". *Earthquake Engineering and Structural Dynamics*, 35(9), 1167-1185.

[8] Chou, C., Wang, Y., & Chen, J. (2008). "Seismic design and behavior of post-tensioned steel connections including effects of a composite slab". *Engineering Structures*, 30(11), 3014-3023.

[9] Hulsey, A.M. (2016), *Mitigating local buckling of Post-tensioned connections in steel self-centering moments resisting frames*. Thesis, University of Texas at Austin, Austin, TX.

[10] Kim, H-J., Christopoulos, C. (2009). "Numerical models and ductile ultimate deformation response of post-tensioned self-centering moment connections". *Earthquake Engineering and Structural Dynamics*. 38:1-21.

[11] Moradi, S., and Alam, S. (2015). "Finite-element simulation of posttensioned steel connections with bolted angles under cyclic loading". *Journal of Structural Engineering*, 142(1), 0733-9445.

[12] Ahmadi, O., Ricles, J. M., and Sause, R. (2018). "Modeling and seismic collapse resistance study of a steel SC-MRF". *Soil Dynamics and Earthquake Engineering*, 113,324-338.

[13] ABAQUS. Inc., ABAQUS Analysis User's Manual, v. 6.13; 2013.

[14] Ricles, J., Sause, R., Peng, S.W., and Lu, L.W. (2001). "Experimental evaluation of earthquake resistant posttensioned steel connections". *Journal of Structural Engineering*, 128(7), 850–859.

[15] AISC 341. (2010). *Seismic provisions for structural steel buildings*. Chicago, IL: American Institute of Steel Construction.

[16] Esposto, M. (2009). *PTED beam-to-column connections for steel moment resisting frames: structural identification based on numerical analysis*, Doctoral Dissertation, Università degli Studi di Napoli Federico II, Naples, Italy.